



1 **Bringing Microphysics to the Masses: The Blowing Snow Observations at the University of**
2 **North Dakota: Education through Research (BLOWN-UNDER) Campaign**

3 Aaron Kennedy¹, Aaron Scott¹, Nicole Loeb², Alec Szczepanski¹, Kaela Lucke¹, Jared Marquis¹,
4 Sean Waugh³

5 *1. Dept. of Atmospheric Sciences, University of North Dakota, Grand Forks, North Dakota*

6 *2. Department of Environment and Geography, University of Manitoba*

7 *3. NOAA National Severe Storms Laboratory, Norman, Oklahoma*

8 **Abstract**

9 Harsh winters and hazards such as blizzards are synonymous with the northern Great Plains
10 of the United States. Studying these events is difficult; the juxtaposition of cold temperatures and
11 high winds makes microphysical observations of both blowing and falling snow challenging.
12 Historically, these observations have been provided by costly hydrometeor imagers that have been
13 deployed for field campaigns or at select observation sites. This has slowed the development and
14 validation of microphysics parameterizations and remote-sensing retrievals of various properties.
15 If cheaper, more mobile instrumentation can be developed, this progress can be accelerated.
16 Further, lowering price barriers can make deployment of instrumentation feasible for education
17 and outreach purposes.

18 The Blowing Snow Observations at the University of North Dakota: Education through
19 Research (BLOWN-UNDER) Campaign took place during the winter of 2019-2020 to investigate
20 strategies for obtaining microphysical measurements in the harsh North Dakota winter. Student
21 led, the project blended education, outreach, and scientific objectives. While a variety of in-situ
22 and remote-sensing instruments were deployed for the campaign, the most novel aspect of the

Corresponding author address: Aaron Kennedy, Department of Atmospheric Sciences, University of North Dakota, 4149 University Ave.,
Box 9006, Grand Forks, ND 58202-9006. E-mail: aaron.kennedy@und.edu

Early Online Release: This preliminary version has been accepted for publication in *Bulletin of the American Meteorological Society*, may be fully cited, and has been assigned DOI 10.1175/BAMS-D-20-0199.1. The final typeset copyedited article will replace the EOR at the above DOI when it is published.

23 project was the development and deployment of OSCRE, the Open Snowflake Camera for
24 Research and Education. Images from this instrument were combined with winter weather
25 educational modules to describe properties of snow to the public, K-12 students, and members of
26 indigenous communities through a tribal outreach program. Along with an educational deployment
27 of a Doppler on Wheels mobile radar, nearly 1000 individuals were reached during the project.

28 **Capsule**

29 A student-led campaign tests more affordable ways of observing blowing and falling snow.
30 Microphysical observations made during the project created a natural bridge between research and
31 outreach objectives.

32 **1. Motivation**

33 Harsh winters and hazards such as blizzards are synonymous with the northern Great Plains
34 of the United States. The earliest records of the challenges these conditions posed on locals come
35 from Plains Indian tribes like the Lakota who recorded their history via pictographs in winter
36 counts (waniyetu wówapi) on mediums such as animal hides (Greene and Thornton 2007; Therrell
37 and Trotter 2011; Howe 2015). Extending for over 100 years in some cases, these historical records
38 documented events such as significant snowfalls, animal deaths due to cold weather, and floods
39 from ice dam breaks. As westerners settled the region in the 1800s, they too were met with the
40 ferocity of winter with stories such as the winter of 1880/81 (Wilder 1940; Boustead 2014;
41 Boustead et al. 2020), the Children's Blizzard in 1888 (Laskin 2005), and the sacrifice of Hazel
42 Miner to save her siblings during a blizzard in 1920 (Kremer 2015), permeating regional culture.

43 Fast forwarding to present day, advancements in science have improved our understanding
44 of blizzards and the underlying processes of falling and blowing snow. From pattern recognition

45 of these events using reanalyses (Kennedy et al. 2019), to satellite and radar- based detection of
46 the hazard (e.g., Palm et al. 2011; Kennedy and Jones 2020), to empirical techniques of predicting
47 blowing snow (Baggaley and Hanesiak 2005; NOAA 2020), a variety of tools now exist to aid
48 forecasters with forecasting winter hazards in this region.

49 Despite these advancements, forecasting blowing and falling snow is an imperfect science.
50 While blizzards are often thought of as the juxtaposition of wind and significant falling snow, these
51 events can also occur without active precipitation. Coined ground blizzards (Stewart et al. 1995;
52 Kapela et al. 1995), these events can have impressive spatial heterogeneity (Kennedy and Jones
53 2020), and are dependent on nuances of the land surface and atmosphere including snowpack age,
54 temperature, and wind speed (Li and Pomeroy 1997a,b; Baggaley and Hanesiak 2005). Because
55 significant snowfall is not expected with ground blizzards, they can take individuals by surprise,
56 and stories of stranded travelers are a common news headline in the region during the winter.

57 Operational models should include parameterizations for blowing snow, but measurements
58 in both time and space are lacking to develop and evaluate such schemes. The cold temperatures
59 and strong winds associated with either type of blizzard make observations challenging.
60 Furthermore, blowing snow events can be difficult to anticipate given sparse observations of the
61 snowpack leading up to these events. Simply measuring snowfall is difficult as noted in winter
62 precipitation testbeds (e.g., Rasmussen et al. 2012) and this poses downstream impacts on blizzard
63 forecasting. Most societal impacts revolve around visibility, with both falling and blowing snow
64 contributing to extinction of light. Given the difficulties in representing this variable through
65 modeling, visibility is an imperfect variable for assessment of event processes and hazards.
66 Instead, direct microphysical measurements are needed and the presence of falling and/or blowing
67 snow requires instrumentation that can measure particles ranging from 10 to 10⁴ μm.

68 A number of techniques have been developed to measure microphysical properties at the
69 surface. While a full survey is beyond the scope of this article, observations range from manual
70 inspection of particles with microscopes (e.g., Shimizu 1963) or cellphones (Kumjian et al. 2020)
71 to instruments that use visible and near-infrared light to obtain properties such as size, shape, and
72 number concentration. Laser-based instruments including the snow-particle counter (SPC;
73 Schmidt 1977; Sato et al. 2017) and the OTT Particle Size Velocity Disdrometer (Parsivel²;
74 Löffler-Mang and Joss 2000; Tokay et al. 2014) can measure particle size distributions (PSDs),
75 while optical imagers including the 2D Video Disdrometer (2DVD; Schönhuber et al. 2007), the
76 Snow Video Imager (SVI, Newman et al. 2009), the Precipitation Imaging Package (PIP; Pettersen
77 et al. 2020), and the Multi-Angle Snowflake Camera (MASC; Garrett et al. 2012) provide images
78 that can be used to derive PSDs and determine particle phase/habit. These observations have also
79 been acquired via ground deployment of aircraft optical probes such as the Cloud Particle Imager
80 (CPI; Lawson et al. 2001; Lawson et al. 2006). Other devices such as manual snow traps (Mellor
81 and Radok 1960) and the acoustic FlowCapt (Chritin et al. 1999) can observe bulk properties such
82 as mass flux of blowing/drifted snow.

83 While these instruments have many strengths, several broad weaknesses exist.
84 Microphysical observations are generally expensive compared to other in-situ atmospheric
85 measurements. For example, temperature sensors are typically < \$1000 USD while aircraft probes
86 can cost > \$100K USD. This limits deployments to specific sites or for limited field campaigns.
87 While the cost is justified due to the complexity and limited market for these instruments, it poses
88 a barrier that 1) slows science and 2) hampers their widespread use for educational and outreach
89 objectives. Further, many of the current instruments are flawed when it comes to sampling
90 snowfall or blizzard environments. Accurate sizing of a broad range of particles during falling or

91 blowing snow events is an issue for instruments like the Parsivel² (Battaglia et al. 2010; Loeb and
92 Kennedy 2021) while instruments with enclosed sampling volumes like the MASC raise the
93 likelihood of interactions with the environmental wind field (Fitch et al. 2021). Other instruments
94 such as the PIP are not commercially available. In light of these issues, affordable microphysics
95 instrumentation capable of operating in snowfall or blizzard environments needs to be developed
96 and tested. Further, these designs should be of open nature like the SVI or PIP to minimize wind
97 effects.

98 The Blowing Snow Observations at the University of North Dakota: Education through
99 Research (BLOWN-UNDER) Campaign took place during the winter of 2019-2020 to investigate
100 strategies for attaining microphysical measurements in harsh winter environments. This project
101 served as the first real world test for OSCRE, the Open Snowflake Camera for Research and
102 Education. OSCRE was deployed throughout the winter, collecting 93 hours of observations across
103 19 different precipitation and blowing snow events. Recorded events ranged from 0.5 to 12 hours
104 of observation time with a mean and standard deviation of 4.9 ± 3.8 hours. An intensive operation
105 phase (IOP) of the project was held from 20 January – 13 February 2020 to coincide with an
106 educational deployment of a Center for Severe Weather Research Doppler on Wheels (DOW7).
107 The project also tested the recently upgraded balloon-borne Particle Size and Velocity (PASIV)
108 probe (Waugh et al. 2015). While the IOP period was generally quiescent, the campaign concluded
109 with a classic ground blizzard on 12 February 2020.

110 The purpose of this article is to highlight OSCRE and the BLOWN-UNDER campaign.
111 The entwinement of science, education, and outreach objectives of the project are emphasized.
112 Preliminary data from the 12 February 2020 ground blizzard are presented throughout to highlight
113 the success of the campaign. The article concludes with lessons learned from the experience.

114 **2. Developing OSCRE**

115 OSCRE takes design cues from the PIP and PASIV to create an affordable hydrometeor
116 imaging system for ground deployments. Major components of the system include a USB3
117 machine vision camera and lens, a computing platform that controls the camera, and a strobed
118 LED light triggered by output from the camera. Collectively, the system is capable of resolving
119 hydrometeors down to $\sim 50 \mu\text{m}$ in diameter. Components are housed within commercially available
120 heated housings and mounted to a simple, treated lumber platform (Figure 1). A full list of
121 components and approximate prices at time of publication are listed in Table 1. The open design
122 of the instrument, parts lists and instructions are provided at:
123 <https://github.com/KennedyClouds/OSCRE>. Details on the imaging system are provided in the
124 sidebar.

125 *a) Design*

126 Compared to other systems, OSCRE is unique in its use of affordable strobed lighting to
127 ‘freeze’ hydrometeors as they pass through the frame. The system uses a Smart Vision Lights
128 ODS75 brick light with narrow lenses to strobe the sampling volume. A singular light is aimed
129 from the side and slightly forward of the focal plane (Figure 1a and c). This is adequate to image
130 hydrometeors at an exposure time of 5-10 μs at a distance of $\sim 20 \text{ cm}$. A major advantage of this
131 light is an internal controller that greatly simplifies the triggering process. The strobe is activated
132 by a pulse generator on the camera or simply when the exposure is occurring. While the system is
133 effective, strobing at visible wavelengths can cause issues with individuals with light sensitivity.

134 Weatherproofing is a challenge for any instrument. To handle harsh winter conditions,
135 OSCRE uses two, IP66 rated dotworkz ST-RF-MVP camera housings. These units include 65 W

136 internal heaters with a blower unit supporting temperatures down to -60°F . While temperatures to
137 this extreme were not observed during BLOWN-UNDER, the system had no issues handling
138 conditions down to -20°F , and no downtime was caused due to weather. An additional benefit of
139 these housings is included 12/24 V output adequate to power the camera and computer ($< 20\text{ W}$).
140 A separate power supply is needed for the lighting due to the draw needed during individual
141 strobes.

142 The final complexity of developing instrumentation is connectivity of equipment. To avoid
143 the expenses with machining, the current generation of OSCRE relies on 3D printed parts created
144 with OpenSCAD (Figure 1d). The project uses an open hardware lens mount modified with a base
145 plate to attach it to the dotworkz housing. An additional bracket and clip were created to hold the
146 Xavier NX within the housing. A 3D printed bracket or duct sealing putty is adequate to keep the
147 light in place. Cabling includes power into each housing and Ethernet into the computer (although
148 wireless can also be used). The most complex part of the system is 5-6pin output wiring between
149 the light, camera, and external power. This requires a pull-up resistor to activate the strobe with
150 the output wire.

151 *b) Example imagery*

152 The 2019-2020 winter was a perfect test period for OSCRE featuring a wide range of
153 precipitation events from October to May. During this period, the system used a JAI 2.3 MP
154 machine vision camera at a focal length of 0.8 m (Figure 1a), yielding an effective resolution of
155 $\sim 28\ \mu\text{m}/\text{pixel}$ for the images shown in Figures 2-3. Exposure times ranged from 6-10 μs at a rate
156 of 30 fps.

157 Multiple blizzards were sampled, including a Colorado low event with significant falling
158 and blowing snow on 28-30 December 2019 and a ground blizzard forced by an Arctic front on 12
159 February 2020¹. OSCRE images during blowing snow are characterized by a large number of ice
160 crystals with maximum dimensions typically < 1 mm (Figure 2). Although scenes were
161 predominately shattered and rounded ice crystals (~100 were identified in Figure 2a), larger
162 hydrometeors were occasionally seen such as a 1.7 mm hexagonal plate (Figure 2a) and a 4.4 mm
163 broken dendrite (Figure 2b). These images also demonstrate a limitation of the current lighting
164 system; even with narrow optics, the lighted volume is deeper than the DoF. This led to a large
165 number of out of focus hydrometeors, necessitating image processing schemes that require contrast
166 detection. Part of this issue was resolved by switching to a FLIR camera with a smaller sensor.
167 This allows for equivalent resolution but at a longer focal length, nearly doubling the DoF.

168 Besides blizzards, OSCRE sampled a wide variety of snowfall and mixed-phase events
169 (Figure 3). On 15 December 2019, a light snow event occurred with a near saturated, boundary
170 layer temperature profile within the dendritic growth zone (DGZ, $-15 \pm 5^\circ$ C). Not surprisingly,
171 snowflake habit featured a number of fern and stellar dendrites along with simple stars (Figure 3a).
172 Broken dendrites were also seen along with growth around rimed cores. Some aggregation was
173 observed, with the largest ~1 cm in length. Note that the singular viewing angle for OSCRE (unlike
174 MASC) can occasionally lead to needle-like shapes due to snowflakes being imaged parallel to
175 their primary face.

176 Prior to blizzard conditions being reached during the 12 February 2020 event, OSCRE
177 sampled pre-frontal snow (Figure 3b). Conditions during this period were much warmer with lack

¹ Descriptions of these blizzard causing systems are provided in Kennedy et al. (2019).

178 of a DGZ. Habit was predominately irregular aggregates with various extents of riming. In the
179 thirty minutes leading up to the frontal passage at ~0730 UTC, there was a noticeable change in
180 habit to fewer aggregates and rimed snowflakes.

181 The final highlighted event is a mixed-phase event on 2 April 2020 (Figure 3c). With
182 conditions near freezing, the event started with a variety of hydrometeors at the surface including
183 rain (3 dotted structures due to reflection/refraction of light), partially and fully frozen drops
184 including spicules, and melted snowflake structures. As the event progressed, there was a rapid
185 change to large aggregates with the largest having a maximum diameter > 4 cm (this structure
186 extended out of frame). The duration of large aggregates was short-lived with later habits featuring
187 smaller aggregates and individual snowflakes with riming.

188 **3. BLOWN-UNDER: Students lead the way**

189 BLOWN-UNDER took lessons learned from the first author during their experience as a
190 graduate student associated with the Student Nowcasting & Observations of Winter Weather with
191 the DOW at University of North Dakota Education in Research (SNOWD UNDER) campaign held
192 in 2010 (UCAR 2020). Similiarly, BLOWN-UNDER was designed by students. An initial kick-
193 off meeting identified goals and broke the project into five teams (Table 2). Each team was led by
194 a graduate student and appropriate operations and safety plans were created. This provided
195 structure to the campaign, gave graduate students leadership experience, and facilitated
196 communication throughout the group. Undergraduate and other interested graduate students were
197 assigned to groups based on interest. The project involved five graduate student leaders and an
198 additional 19 undergraduates and graduate students assigned to teams. A few additional individuals

199 assisted with other aspects of the campaign such as educational outreach and the 12 February 2020
200 IOP.

201 *a) Science goals and observations during blizzard events*

202 The primary science goals of the campaign were to characterize micro- and macrophysical
203 properties and boundary layer structure and evolution during blizzard and blowing snow events.
204 The strengths and weaknesses of deployed instruments (including OSCRE) were also explored to
205 guide future field work. A list of instruments partitioned by team is provided in Table 2.

206 Surface instrumentation included standard meteorological observations from a mesonet
207 site and DOW7, and microphysical information from an OTT Hydromet Parsivel² and the OSCRE.
208 The latter two instruments were deployed to provide microphysical ground truth (PSDs) and to
209 help segregate between falling/blowing snow. A loaned North Dakota Agricultural Network
210 mesonet with a 3 m tower was collocated with the ceilometer and Parsivel² at the Oakville Prairie
211 Observatory located ~13 miles west of Grand Forks, North Dakota, near the Grand Forks Air Force
212 Base. Limited bandwidth at this location along with the experimental nature of OSCRE led to
213 deployment of this instrument within Grand Forks, ND.

214 Remotely-sensed observations included both radar and lidar assets. A Lufft CHM 15k 1064
215 nm laser ceilometer was loaned to the project from OTT Hydromet. Providing vertical profiles of
216 attenuated backscatter, deployment allowed for surface-based detection of blowing snow layers
217 similar to studies in Antarctica (Gossart et al. 2017; Loeb and Kennedy 2021).

218 Core instrumentation such as the ceilometer sampled blowing snow layers during several
219 blizzards to varying degrees of success (Figure 4). During and after an extended period of falling
220 snow, blizzard conditions were reached from 1500-0200 UTC 29-30 December 2019 (Figure 4a).

221 Blowing snow is easily identified by the near-surface maximum of backscatter throughout the
222 period with layer heights around 300-400 m. Fall streaks and cloud structures above the blowing
223 snow layer were also present suggesting the ceilometer was not significantly attenuated by the
224 blowing snow.

225 Greater measurement difficulty for the ceilometer was found with the 12 February 2020
226 ground blizzard (Figure 4b). Meteorologically, this event was forced by an intense Arctic front.
227 Over the course of minutes, wind magnitude increased from 7 to 20 m s⁻¹. The strong winds
228 combined with recent pre-frontal snowfall led to a wall of darkness (whiteout conditions) as seen
229 by area cameras (not shown). This frontal passage is easily seen in the ceilometer data by a rapid
230 increase in backscatter in the lower 200 m of the profile at 0715 UTC. After a couple of hours of
231 intense near-surface backscatter extending up to ~500 m, the blizzard was strong enough to limit
232 penetration to only the lowest several range bins (<50 m). Blowing snow layer heights were only
233 retrievable as the event subsided (17 UTC). In this and other cases, temporal fluctuations in
234 ceilometer backscatter were present, indicative of horizontal convective rolls containing blowing
235 snow (Kennedy and Jones 2020). Further, most events concluded with backscatter first
236 diminishing near the surface as winds decreased, and then a gradual reduction of intensity within
237 a suspended blowing snow layer.

238 Radars are also capable of detecting blowing snow events (Vali et al. 2012; Geerts et al.
239 2015; Kennedy and Jones 2020; Loeb and Kennedy 2021), although exact sensitivity limits are
240 unknown. To provide mesoscale details and understand detection limits, dual polarized
241 observations were made at X (DOW7, <https://dowfacility.atmos.illinois.edu/>), C (UND NorthPOL,
242 <http://radar.atmos.und.edu/>) and S (KMXW WSR-88D, <https://www.roc.noaa.gov/WSR88D/>)
243 bands. Scanning strategies between DOW7 and NorthPOL were coordinated during the 12

244 February 2020 blizzard including synced scans between the radars. Deployment locations for
245 DOW7 were identified in advance to minimize issues with beam blockage and allow for Dual-
246 Doppler lobes with either NorthPOL or KMVX.

247 Example radar data from 0840 UTC during the 12 February 2020 blizzard is provided in
248 Figure 5. The location of the front (now south of the campaign location) is seen as a fineline in
249 KMVX data (Figure 5c). Immediately behind the pre-frontal snow and cold front are horizontal
250 convective rolls of blowing snow near DOW7 and KMVX (Figures 5a and c). Oriented
251 approximately north to south with the mean boundary layer wind vector, these shallow features
252 are associated with increased reflectivity and variability in the velocity field (not shown). As the
253 event progressed, these features took on an elongated and more regularly spaced appearance
254 typical of other events (Kennedy and Jones 2020). While falling snow was also viewed by
255 NorthPOL, clutter issues in the lowest layers (within city limits) prevented detection of the
256 horizontal convective rolls (Figure 5b). The shallow nature of the blowing snow layer (~400-500
257 m as detected by radar) means that detection was limited to 10s of km from radar sites at the lowest
258 usable elevation tilts.

259 Two types of sondes were launched during BLOWN-UNDER with GRAW DFM-09
260 radiosondes providing wind, temperature, humidity, and pressure observations while the PASIV
261 provided vertical profiles of PSDs (Figure 6). The campaign used an upgraded version of the 1st
262 generation PASIV (Waugh et al. 2015). The new version uses a 4112x3008 pixel Ximea
263 MC124CG-SY machine vision camera powered by an Nvidia Jetson TX2 computer. With a
264 sampling volume of 29x20x11.5 cm, the system is capable of resolving hydrometeors > 100 μ m
265 in diameter at a rate of ~20 frames per second. The weight of the PASIV (just under the U.S.
266 Federal Aviation Administration regulation Part 101 limit of 2.72 kg) necessitated a large amount

267 of helium (two 200 HE cylinders; 11.3 m³) per launch. Due to a regional helium shortage during
268 the campaign, only two launches were made (6 February 2020 and 12 February 2020). Because
269 the PASIV does not actively transmit data, probes were retrieved with aid of a SPOT GPS tracker
270 (Figure 6b and c).

271 Ballooning is notorious for adventures, and BLOWN-UNDER was no exception. The 6
272 February 2020 launch did not use a cut-down mechanism and travelled far enough to land in a
273 forested recreational area near Fertile, MN (Figure 6b). Unfortunately, the data disk became loose
274 during launch and no hydrometeor information was recorded. Issues with the cut-down device and
275 security of the drive were fixed by 12 February 2020, and a launch in pre-frontal snow was made
276 at 0640 UTC. Given the close proximity of recovery and expected winds behind the front, the
277 decision was made to retrieve the device prior to the frontal passage. While this was achieved
278 (Figure 6c), retrieval was delayed due to the need to snowshoe into a field. On the way back to
279 town, the recovery team including the first author was hit by the frontal passage and ended up
280 stuck in open country until conditions improved ~8 hours later. An important safety lesson was
281 learned, but PASIV data were successfully recovered (Figure 6d).

282 *b) Communications*

283 Communications for the project varied before and during the DOW7 deployment window.
284 Leading up to the campaign, communications were traditional, using email and surveys to build
285 teams and schedule meetings. During the IOP period, communication was maintained using daily
286 weather briefings and the popular, freeware instant messaging application, Discord (Figure 7).
287 While the use of Discord has been noted in educational environments (Lacher and Biehl 2018;

288 Fonseca Cacho 2020), the authors are unaware of formal publications documenting use of Discord
289 for field campaigns.

290 Highlighting the use of Discord, this activity was considered a success. The ability to create
291 multiple channels to support specific teams decluttered communications. Support for pictures and
292 videos was extensively used to share real-time data (e.g., DOW7 and sounding data). Finally,
293 instant-messaging was used to contact specific users. Because Discord is supported in web
294 browsers as well as OS specific applications, it was easily accessible to campaign participants.
295 While not used, the ability to program bots could be advantageous in the future (e.g., querying
296 real-time data from observations). While virtually all of these features are also available in the
297 Slack platform, it's worth noting that Discord is more commonly used by students due to its
298 presence in online gaming communities.

299 *c) Forecast and Modeling Activities*

300 Local noon (18 UTC) weather briefings were prepared by the student forecasting team each
301 weekday of the campaign. Students met to view real-time observations and model output to
302 produce a forecast for the next three days. If the possibility of falling or blowing snow was
303 identified, the entire team was put on alert and additional times (e.g., the weekend) were identified
304 for team members to be on call. During IOPs, team members kept others updated on conditions
305 via Discord.

306 Besides the standard suite of operational models, forecasters also had access to Weather
307 Research and Forecasting (WRF) model simulations designed by the team. These simulations were
308 run daily at 00 and 12 UTC on a local cluster. Students prioritized resolution and chose a 3 km
309 inner nest, and output was tailored to the project including appropriate variables (visibility) from

310 the Air Force Weather Agency (AFWA) and contouring intervals appropriate for the time period.
311 To show the absence of blowing snow in WRF and its impacts on forecast visibility, a column
312 blowing snow model, PIEKTUK (Déry and Yau 2001b), was implemented in Python and forced
313 by WRF output.

314 Observation based analyses and WRF output valid at 0900 UTC 12 February 2020 during
315 the ground blizzard component of the event are shown in Figure 8. The location of the southward
316 moving Arctic front is easily identifiable by the gradient in temperature, and presence of strong
317 northerly winds behind the front (Figure 8a and b). Visibility reductions due to falling snow were
318 present along the front in both observations and WRF AFWA output (Figure 8a and c). More
319 significant reductions in visibility occurred behind the front due to blowing snow; the lack of this
320 process in WRF led to no reductions in visibility for this region (Figure 8c). PIEKTUK on the
321 other hand, showed reduced visibilities behind the front where wind speeds were sufficiently
322 strong to trigger the column blowing snow model (Figure 8d). While this is an encouraging result,
323 it is noted that impacts were too widespread. In this case, blowing snow did not occur where little
324 to no snow fell leading up the frontal passage. This highlights the ongoing work needed to improve
325 blowing snow modeling before it is widely included within mesoscale models.

326 **4. Connecting research to outreach**

327 The widespread impacts of winter weather on the northern Great Plains make the subject a
328 perfect topic for outreach. A number of activities were carried out before and during the BLOWN-
329 UNDER campaign. Approximately 1000 individuals were reached during the 2019-2020 winter
330 across a tribal college outreach program, a STEM café at a local brewery, school visits, and
331 science/community days in the region (Table 3). The quiescent start to the campaign allowed for

332 more visits with DOW7 than otherwise expected, and one day was set aside for the radar to visit
333 the Little Hoop Tribal Community College within the Spirit Lake Reservation.

334 A core component of outreach was the development of hands-on activities to engage
335 participants (Figure 9). Learning objectives included discovery of snow properties, identifying
336 whether it can be blown, and understanding how light interacts with ice crystals. Several of these
337 activities are now described.

338 **Blizzard in a box:** Two types of artificial snow were acquired including finely ground
339 plastic shavings and a water absorbent polymer. These represent snowfall events with low and
340 high liquid water content, respectively. After students felt each type of snow, they were encouraged
341 to think about how this impacts real-world experiences such as creating snowballs or shoveling
342 snow. They were then asked which one is more likely to be blown by the wind. A handheld fan
343 was then used to (unsuccessfully) blow the wet snow. The activity then shifted to an aquarium that
344 held the dry, plastic-based artificial snow (Figure 9a). Participants created LEGO creations to serve
345 as obstacles. With the tank mostly covered, students then used the handheld fan to create a blizzard.
346 After the wind subsided, students were asked about snow drifts and how this impacts the
347 measurement of snowfall. Depending on the age level, this activity was a qualitative or quantitative
348 exercise, but the end result was a better understanding of how obstacles and drifts impact snowfall
349 measurements.

350 **Atmospheric optics:** Sun dogs, light pillars, and other more complex halos are a common
351 occurrence in the region. To teach individuals about the concepts of reflection and refraction, 3-D
352 printed hexagonal plate crystals were created with a resin 3D printer (Figure 9b). After the crystals
353 were printed, they were sanded down to 2000-grit, then coated in clear automotive enamel. The

354 result is an almost completely transparent, custom made prism. Students used a flashlight to see
355 the processes of refraction and reflection. In practice, the crystals will reflect light upwards or
356 downwards off the face (responsible for light pillars) and refract light at an angle to produce sun
357 dogs (parhelia).

358 Snowflake habit matching and art: 3D printers were used to create specific snowflake
359 habits (plates, aggregates, bullet rosettes, columns, etc.) to teach individuals about the variability
360 of ice habits and environments they form in (Figure 9c and d). Printed crystals were matched to a
361 graphic table of habits, and real-world examples were shown from OSCRE. A Thingiverse project
362 (The Snowflake Machine by user mathgrrl) was used to create randomly generated dendrites.
363 These were handed out to students to use for art rubbings and were allowed to be taken home as
364 gifts.

365 Hands-on activities were also packaged into a complete winter weather module for the
366 Nurturing American Tribal Undergraduate Research and Education (NATURE) Sunday Academy
367 outreach program. The authors travelled to five tribal colleges throughout the fall and winter and
368 presented to high school students at their respective reservations. Topics of the unit included a
369 cultural connection activity (e.g., a history of winter counts) taught by a tribal liaison, and various
370 winter weather lessons ranging from winter safety tips to reading weather maps and identifying
371 the type of weather systems responsible for blizzards in the region. Hands-on activities were mixed
372 throughout the lesson to provide engagement. Formal assessment for the program was positive
373 with a mean rating of 3.87 out of 5.0 (with 1 = Poor, 5 = Excellent) for overall quality of the lesson.
374 Other questions asked about how interesting the topic was (3.76), the extent hands on activities
375 added to lesson quality (3.09), and the extent to which Native American culture and the science
376 topic were related (2.85). Students highlighted the hands-on activities, and suggestions for

377 improvement included adding more of these activities. To improve the cultural connection score,
378 future iterations should mix these activities throughout the event vs. having a stand-alone section
379 at the beginning.

380 **5. Summary and Lessons Learned**

381 While blizzards are common in the region, there is no guarantee weather will cooperate for
382 field campaigns, especially those with short time windows such as educational deployments. An
383 active winter ensured OSCRE had plenty of events to sample throughout the winter, but most of
384 the BLOWN-UNDER IOP period was quiet. This time was instead used to exceed expectations
385 for outreach. Regarding science objectives, the ground blizzard of 12 February 2020 was a
386 homerun event by every measure, ensuring these goals were also met. The combination of in-situ
387 and remotely-sensed observations of the event will offer an unprecedented look into the evolution
388 of a ground blizzard, and a detailed case study is the subject of forthcoming work.

389 Moving forward, a number of lessons were learned that will guide future deployments for
390 blizzard research. Regarding observations during BLOWN-UNDER:

- 391 • Importance of winterizing equipment: While DOW7 performed admirably for the event,
392 exposure and cold took its toll as blowing snow was ingested into various components of
393 the system, eventually leading to failure of the generator powering the radar. The cold also
394 led to the hydraulic mast freezing, leaving DOW7 in place until it could be loosened (Figure
395 10).
- 396 • The dynamic landscape of cold-regions: While deployment locations were scouted in
397 advance for DOW7, anthropogenic piles of snow and natural drifts led to surprises. Time
398 must be set aside prior to events to identify ideal locations for mobile assets.

399 • The difficulty and safety of PASIV launches. The weight of the current PASIV necessitates
400 a large balloon that uses two HE 200 cylinders of helium. This weight is still sufficiently
401 light with a large surface area that makes launches in windy environments challenging
402 (e.g., the instrument can be difficult to hold in high winds). Weight savings can be sought
403 to reduce the overall size of the instrument and thus reduce the complexity in launching.
404 Additionally, a reduction in weight would also reduce the helium required for lift. Further,
405 the PASIV can be modified for missions that are focused on the near-boundary layer,
406 maximizing the residence time in the region of interest rather than the entire troposphere
407 as originally designed. Finally, key components should be ruggedized so there is no need
408 or desire to retrieve probes immediately. This will ensure the safety of participants as
409 launches can be made near heated locations where cold exposure is kept to a minimum.
410 Participants that help with retrievals after events conclude should be provided training
411 regarding cold weather attire, and retrieval methods such as snowshoeing.

412 Regarding the development and deployment of OSCRE:

413 • Feasibility of affordable microphysical measurements: OSCRE has demonstrated that habit
414 and size can be obtained in nearly any cold-season environment. The price point is
415 significantly less than commercial options suggesting networks could be implemented to
416 understand spatial and temporal variability of falling and blowing snow.

417 • Computing limitations: Making OSCRE affordable necessitated a number of design
418 sacrifices such as brute-force imaging and off-the-shelf components. Current hardware
419 does not support retrieval of fall speeds, but affordable advancements in cameras and
420 computing may make this possible in the future. In its present form, OSCRE is capable of

421 handling IOP style deployments, but long-term, unattended use will be possible with
422 further code development.

- 423 • Lighting: Current lighting is sufficient for imaging hydrometeors but the sampling volume
424 may be impacted by flow around the instrument. Current lighting has too much spread and
425 this leads to the use of contrast-detection methods to identify in-focus hydrometeors. The
426 lighting system needs further refinement to let the light define the sampling volume. This
427 will simplify hydrometeor detection and may make analysis of hydrometeors feasible in
428 real-time. A housing could be developed to minimize flow disruptions and increase the
429 intensity of light, but this will most likely increase the costs of the system.

430 **Acknowledgements**

431 BLOWN-UNDER was possible due to the support of numerous groups. Funding for the
432 project and outreach efforts was provided by the National Science Foundation (NSF) under AGS
433 #1834748 and NSF EPSCoR Track-1 Cooperative Agreement OIA 1355466. NSF support also
434 included deployment of DOW7 through the NCAR Earth Observing Laboratory (EOL)
435 educational deployment program. The authors thank Joshua Wurman, Karen Kosiba, and radar
436 operator Alycia Gilliland of the Center for Severe Weather Research for their tireless support
437 throughout the campaign. Other individuals that deserve recognition include Victor Cassella of
438 OTT Hydromet who made the ceilometer deployment possible, and Daryl Richardson and James
439 Hyde of the North Dakota Agricultural Network for loaning the mesonet station. The UND
440 Departments of Biology and Space Studies are thanked for allowing use of the Oakville Prairie
441 Field Station and Observatory. Finally, we thank three anonymous reviewers who provided
442 feedback that improved the clarity of this manuscript.

443 **Data Availability Statement**

444 Code and data used to create figures within this manuscript along with OSCRE documentation are
445 available at: <https://github.com/KennedyClouds>.

446

447 **Appendix: Acronyms**

448 Acronyms used in the text are listed here.

449	2DVD	2D Video Disdrometer
450	AFWA	Air Force Weather Agency
451	BLOWN-UNDER	Blowing Snow Observations at the University of North Dakota: Education
452		through Research
453	CMOS	Complementary Metal Oxide Semiconductor
454	CPI	Cloud Particle Imager
455	DoF	Depth of Field
456	DOW	Doppler on Wheels
457	DGZ	Dendritic Growth Zone
458	FoV	Field of View
459	GPU	Graphics Processing Unit
460	IOP	Intensive Operation Phase
461	MASC	Multi-Angle Snowflake Camera
462	NATURE	Nurturing American Tribal Undergraduate Research and Education
463	OSCRE	Open Snowflake Camera for Research and Education
464	Parsivel ²	Particle Size Velocity Disdrometer
465	PASIV	Particle Size and Velocity probe
466	PIP	Precipitation Imaging Package
467	PSD	Particle Size Distribution
468	SNOWD UNDER	Student Nowcasting & Observations of Winter Weather with the DOW at
469		University of North Dakota Education in Research
470	SPC	Snow-Particle Counter
471	SSD	Solid State Drive
472	SVI	Snow Video Imager

474 **References**

Baggaley D. G., and J. M. Hanesiak, 2005: An Empirical Blowing Snow Forecast Technique for the Canadian Arctic and the Prairie Provinces. *Wea. Forecasting*, **20**, 51–62.

Battaglia, A., Rustemeier E., Tokay A., Blahak U., and Simmer C., 2010: PARSIVEL snow observations: A critical assessment. *J. Atmos. Oceanic Technol.*, **27**, 333–344.

Boustead, B. E., 2014: The Hard Winter of 1880–1881: Climatological context and communication via a Laura Ingalls Wilder narrative. Ph.D. dissertation, School of Natural Resource, University of Nebraska–Lincoln, 196 pp.

Boustead, B. M., M. D. Shulski, and S. D. Hilberg, 2020: The Long Winter of 1880/81. *Bull. Amer. Meteor. Soc.*, **101**, E797–E813.

Chritin, V., , Bolognesi R. , , and Gubler H. , 1999: FlowCapt: A new acoustic sensor to measure snowdrift and wind velocity for avalanche forecasting. *Cold Reg. Sci. Technol.*, **30**, 125–133.

Fitch, K. E., Hang, C., Talaei, A., and Garrett, T. J.: Arctic observations and numerical simulations of surface wind effects on Multi-Angle Snowflake Camera measurements, *Atmos. Meas. Tech.*, **14**, 1127–1142, <https://doi.org/10.5194/amt-14-1127-2021>, 2021.

Fonseca Cacho, Jorge, "Using Discord to Improve Student Communication, Engagement, and Performance" (2020). *UNLV Best Teaching Practices Expo*. 95. https://digitalscholarship.unlv.edu/btp_expo/95

Garrett, T. J., C. Fallgatter, K. Shkurko, and D. Howlett, 2012: Fallspeed measurement and high-resolution multi-angle photography of hydrometeors in freefall. *Atmos. Meas. Tech.*, **5**, 2625–2633.

Geerts, B., B. Pokharel, and D. A. R. Kristovich, 2015a: Blowing snow as a natural glaciogenic cloud seeding mechanism. *Mon. Wea. Rev.*, **143**, 5017–5033, doi:10.1175/MWR-D-15-0241.1.

Gossart, A., Souverijns, N., Gorodetskaya, I. V., Lhermitte, S., Lenaerts, J. T. M., Schween, J. H, 2017: Blowing snow detection from ground-based ceilometers: application to East Antarctica. *The Cryosphere*, **11**(6), 2755–2772.

Green C., and R. Thornton, Eds., 2007: The Year the Stars Fell: Lakota Winter Counts at the Smithsonian. University of Nebraska Press, 370 pp.

Howe, C., 2015: Lakota Star Knowledge and Lakota Winter Counts. Lecture presented at Oglala Lakota College, 12 November 2015. Accessed online at: <https://www.youtube.com/watch?v=TEyJraivn8M>

Kapela, A. F., P. W. Leftwich, and R. Van Ess, 1995: Forecasting the impacts of strong wintertime post-cold front winds in the northern plains. *Wea. Forecasting*, **10**, 229–244.

Kennedy, A., and C. Jones, 2020: GOES-16 Observations of Blowing Snow in Horizontal Convective Rolls on 24 February 2019. *Mon Wea Rev*, **148**, 1737–1750.

Kennedy, A. A. Trellinger, T. Grafenauer, and G. Gust, 2019: A Climatology of Atmospheric Patterns Associated with Red River Valley Blizzards, *Climate* 2019, **7**(5), 66.

Kremer, K. 2015, *Angel of the Prairie: The Heroic Story of Hazel Miner During the North Dakota Blizzard Of 1920*. Snow in Sarasota Publishing, Osprey, FL, USA, p. 125.

Kumjian, M. R., Bowley, K. A., Markowski, P. M., Lombardo, K., Lebo, Z. J., & Kollias, P. (2020). Snowflake Selfies: A Low-Cost, High-Impact Approach toward Student Engagement in Scientific Research (with Their Smartphones), *Bull. Amer. Meteor. Soc.*, **101**(6), E917–E935.

Lacher, L., and C. Biehl, 2018: Using discord to understand and moderate collaboration and teamwork. *Proceedings of the 49th ACM Technical Symposium on Computer Science Education*. 1107–1107.

Laskin, D., 2005: *The Children's Blizzard*, 3rd ed.; HarperCollins: New York, NY, USA, p. 336
Lawson, R. P., , B. A. Baker, , C. G. Schmitt, , and T. L. Jensen, 2001: An overview of microphysical properties of Arctic clouds observed in May and July during FIRE.ACE. *J. Geophys. Res.*, **106** , 14989–15014.

Lawson, R. P., B. A. Baker, P. Zmarzly, D. O'Connor, Q. Mo, J.-F. Gayet, and V. Shcherbakov, 2006a: Microphysical and optical properties of atmospheric ice crystals at South Pole Station. *J. Appl. Meteor. Climatol.*, **45**, 1505–1524.

Lawson, R. P., , B. A. Baker, , C. G. Schmitt, , and T. L. Jensen, 2001: An overview of microphysical properties of Arctic clouds observed in May and July during FIRE.ACE. *J. Geophys. Res.*, **106** , 14989–15014.

Li, L., and J. W. Pomeroy, 1997a: Estimates of threshold wind speeds for snow transport using meteorology data. *J. Appl. Meteor.*, **36**, 205–213.

Li, L., and J. W. Pomeroy, 1997b: Probability of occurrence of blowing snow. *J. Geophys. Res.*, **102** (D18) 21955–21964.

Loeb, N. and A. Kennedy, 2021a: Blowing Snow at McMurdo Station, Antarctica During the AWARE Field Campaign: Surface and Ceilometer Observations. *J. Geophys. Res. Atmos.*, **126**, e2020JD033935.

Löffler-Mang, M., and Joss J. 2000: An optical disdrometer for measuring size and velocity of hydrometeors. *J. Atmos. Oceanic Technol.*, **17**, 130–139.

Mellor, M., and U. Radok, 1960: Some properties of drifting snow. *Antarctic Meteorology*, Pergamon Press, Oxford, 333–346.

NOAA, 2020: Winter Storm Severity Index (WSSI) – Product Description Document (PDD). Accessed 2 February 2021, <https://www.wpc.ncep.noaa.gov/wwd/wssi/wssi.php>

Newman, A. J., Kucera P. A., and Bliven L. F., 2009: Presenting the Snowflake Video Imager (SVI). *J. Atmos. Oceanic Technol.*, **26**, 167–179.

Palm, S. P., Yang, Y., Spinhirne, J. D., & Marshak, A., 2011: Satellite remote sensing of blowing snow properties over Antarctica. *Journal of Geophysical Research: Atmospheres*, **116**(D16).

Pettersen, C. and coauthors, 2020: The Precipitation Imaging Package: Assessment of Microphysical and Bulk Characteristics of Snow. *Atmosphere*, **11**, 785.

Rasmussen, R., and Coauthors, 2012: How well are we measuring snow: The NOAA/FAA/NCAR winter precipitation test bed. *Bull. Amer. Meteor. Soc.*, **93**, 811–829.

Sato, T., Kimura, T., Ishimaru, T., & Maruyama, T., 1993: Field test of a new snow-particle counter (SPC) system. *Annals of Glaciology*, **18**, 149–154.

Shimizu, H., 1963: ‘Long prism’ crystals observed in precipitation in Antarctica. *J. Meteor. Soc. Japan*, **41**, 305–307.

Schmidt, R.A. 1977: A system that measures blowing snow. U.S. Dep. Agric. For. Serv. Res. Pap. RM–194.

Schönhuber, M., Lammer G., and Randeu W. L., 2007: One decade of imaging precipitation measurement by 2D-video-disdrometer. *Adv. Geosci.*, **10**, 85–90.

Stewart, R. E., and and Coauthors, 1995: Winter storms over Canada. *Atmos.–Ocean*, **33**, 223–247.

Therrell, M. D., and M. J. Trotter, 2011: Waniyetu Wówapi: Native American Records of Weather and Climate. *Bull. Amer. Meteor. Soc.*, **92**, 583–592.

Tokay, A., Petersen, W. A., Gatlin, P., and Wingo, M., 2013: Comparison of Raindrop Size Distribution Measurements by Collocated Disdrometers. *J. Atmos. Oceanic Technol.*, **30**, 8, 1672–1690

UCAR, 2020: SNOWD UNDER. Accessed 18 Jan. 2020, https://www.eol.ucar.edu/field_projects/snowd-under.

Vali, G., D. Leon, and J. R. Snider, 2012: Ground-layer snow clouds. *Quart. J. Roy. Meteor. Soc.*, **138**, 1507–1525, doi:10.1002/qj.1882.

Waugh, S. M., C. L. Ziegler, D. R. MacGorman, S. E. Fredrickson, D. W. Kennedy, and W. D. Rust, 2015: A balloonborne particle size, imaging, and velocity probe for in situ microphysical measurements. *J. Atmos. Oceanic Technol.*, **32**, 1562–1580.

Wilder, L. I., 1940: *The Long Winter*. Harper Collins Publishers Inc., 352 pp.

Sidebar: The OSCRE Imaging System

Considerations made for the camera and lens included affordability, flexibility, light sensitivity, and output capabilities. Machine vision cameras that incorporated Sony monochrome Complementary Metal Oxide Semiconductor (CMOS) sensors were selected due to noise/light performance, low exposure times, and use of a global shutter. The latter feature is particularly important for minimizing distortion caused by object motion during individual frames. The current generation of OSCRE uses a 3.2MP FLIR BFS-UD32S4M-C camera with a Sony IMX252 sensor capable of a maximum framerate of 118 fps. Exact imaging properties such as resolution and field of view (FoV) are dependent on the matched lens and focal length chosen; this allows customization of the system to the observations desired (e.g., shattered blowing snow particles vs. large aggregate snowflakes).

To minimize issues with distortion and ensure compatibility with future machine vision cameras (that have larger sensor sizes), a Rokinon 135 mm f/2 full-frame lens with manual aperture and focus controls was selected. Matched to the 1/1.8" Sony IMX252 sensor, the 135 mm lens acts as an effective 648 mm (4.8x crop factor) lens with a minimum focal length of 0.8 m. Distortion is < 0.02% due to only the center of the lens being used. At a distance of 0.8 m, the FoV is 34×26 mm resulting in 16.7 μm pixels. A better balance of resolution and FoV occurs at longer focal lengths (e.g., 1.5 m). This increases FoV to 76×57 mm and pixel size to 37 μm. Depth of Field (DoF) is also increased and is on the order of 10s of millimeters (exact DoF is dependent on contrast detection of objects). Microscope test charts at a distance of 1.5 m suggest hydrometeors ~50 μm can be identified, but with equally as large uncertainty due to specular reflection/contrast issues and fore/aft displacement of the hydrometeor.

The system is controlled by a NVIDIA Jetson Graphics Processing Unit (GPU) computer. Initial development began with a Jetson TX2 contained within a heated, weatherproof box (Figure 1b). The current device uses the Xavier NX developer kit, which is small enough to be included in the camera housing (Figure 1b). The Ubuntu operating system is installed on a 32 GB microSD card while a 2 TB Solid State Drive (SSD) is used for recording data. This allows for continuous operation of the camera at a rate of 30 fps for ~6 hours, although greater frame rates are possible if desired. Until real-time GPU-based software is developed, read/write performance is the single greatest factor on time and a quality SSD is required. The system can also be driven by other operating systems if desired; FLIR software runs on Linux, macOS, and Windows platforms.

Table 1. Components and prices for OSCRE. Prices in parenthesis represent aftermarket cost.

Component	Details	Approximate price (As of Mar. 2021)
Camera	FLIR Blackfly S (USB3) BFS-U3-04S2C-CS <ul style="list-style-type: none"> • 3.2MP, 1/1.8" sensor (Sony IMX252 CMOS) • 118fps, global shutter 	\$800
Lens	Rokinon 135mm F/2 for Nikon F mount <ul style="list-style-type: none"> • Requires Fotodiox Nikon F to C-Mount Adapter • Minimum focus distance: 0.8m • manual aperture/focus controls 	\$600
Computer	NVIDIA Xavier NX Developer Kit <ul style="list-style-type: none"> • NVIDIA Volta GPU, 6-core ARM CPU • 8 GB memory 	\$400
Storage	64GB SanDisk Extreme microSDXC (OS) 2TB Samsung 970 EVO Plus SSD M.2 NVMe (Data)	\$350
Lighting	SmartVisionLights ODS75-WHI OverDrive Brick Light <ul style="list-style-type: none"> • Includes power supply + cabling 	\$500
Housings	2 x Dotworkz ST-RF-MVP housings <ul style="list-style-type: none"> • Heated, require AC cable • Significant savings via aftermarket 	\$1300 (\$300)
Cables/Misc	HDMI Dummy Plug 1ft Micro USB 3.0 Cable. A male to Micro B (up angle) + locking screws CAT6 cable	\$50
Misc.	Lumber for structure, mechanical hardware, 3D printed parts, etc.	\$200
Total		\$4200 (\$3200)

Table 2. BLOWN-UNDER teams and respective learning goals, responsibilities, and instrumentation.

Team	Learning Goals and Responsibilities	Instrumentation
Surface	Learn about and operate in-situ and remotely-sensed surface instruments. Maintain field site and keep instruments operational at the Oakville Prairie Observatory.	Lufft CHM-15K ceilometer NDAWN Mesonet OSCRE Parsivel ²
Balloon	Learn how to launch traditional and PASIV balloon packages. Assist with tracking and retrieval of PASIV launches.	GRAW DFM-09 radiosondes PASIV
Radar	Learn about dual-polarimetric radar observations and scanning strategies. Coordinate and operate UND and DOW7 radars.	DOW7 (X-band) Mayville, ND WSR-88D (S-band) UND North-Pol (C-band)
Forecasting	Learn about numerical weather prediction. Gain hands-on experience running WRF and interpreting output from operational models. Provide weather briefings for the project and real-time guidance to the group.	
Media	Learn about reporting and gain video editing experience. Coordinate social media posts and disseminate info to other news agencies.	

Table 3. BLOWN-UNDER outreach events and attendance.

Event	Date	Total	Adults	Kids	(M)	(F)	Under Represented	Special Needs	General Public
NATURE	Various	81	5	76	NA	NA	82	0	0
Hopped up On Science @ Half Brothers Brewing	1/22/20	40	36	4	1	3	NA	NA	40
Holy Family / St Mary's Elementary School	1/23/20	75	6	69	40	29	3	0	6
Thompson K-12	1/28/20	13	1	12	9	3	1	0	1
Sacred Heart K-12	1/30/20	14	3	11	7	3	2	0	3
Little Hoop Tribal Community College	2/4/20	31	31	NA	NA	NA	31	NA	11
Grand Forks Central High School	2/5/20	152	6	146	80	61	36	10	6
Aerospace Community Day (hands-on)	2/8/20	511	237	274	NA	NA	NA	NA	NA
Discovery Elementary School	2/11/20	82	4	78	35	43	9	2	4
Total (All)		999	330	670	187	164	168	12	106

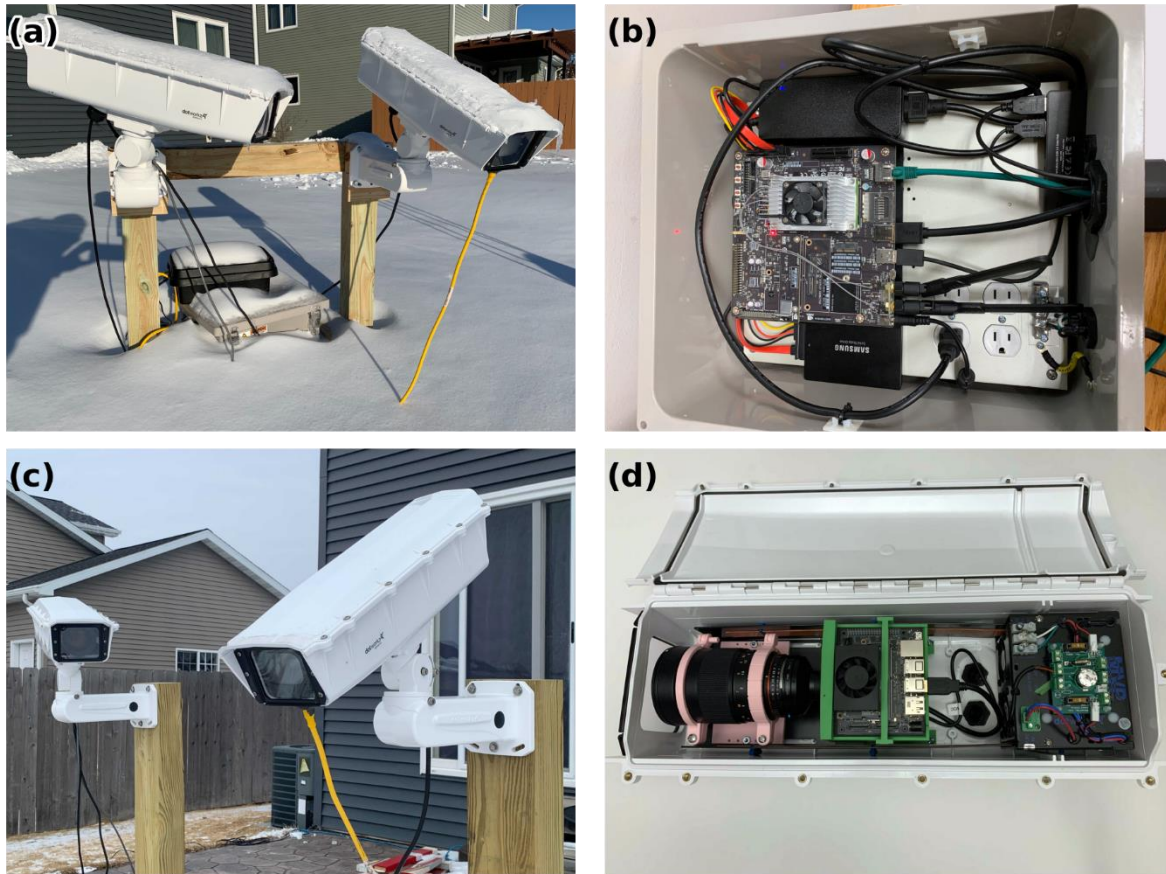


Figure 1. OSCR configurations for the winter of 2019-2020 (a-b) and present day (c-d). Panels (a) and (c) represent focal lengths of 0.8m and 1.5m, respectively. Panel (b) shows the original Nvidia Jetson TX2 contained within an externally mounted heated housing. In panel (d), OSCR is shown with a Jetson Xavier NX mounted internally within the camera housing using 3D printed brackets.

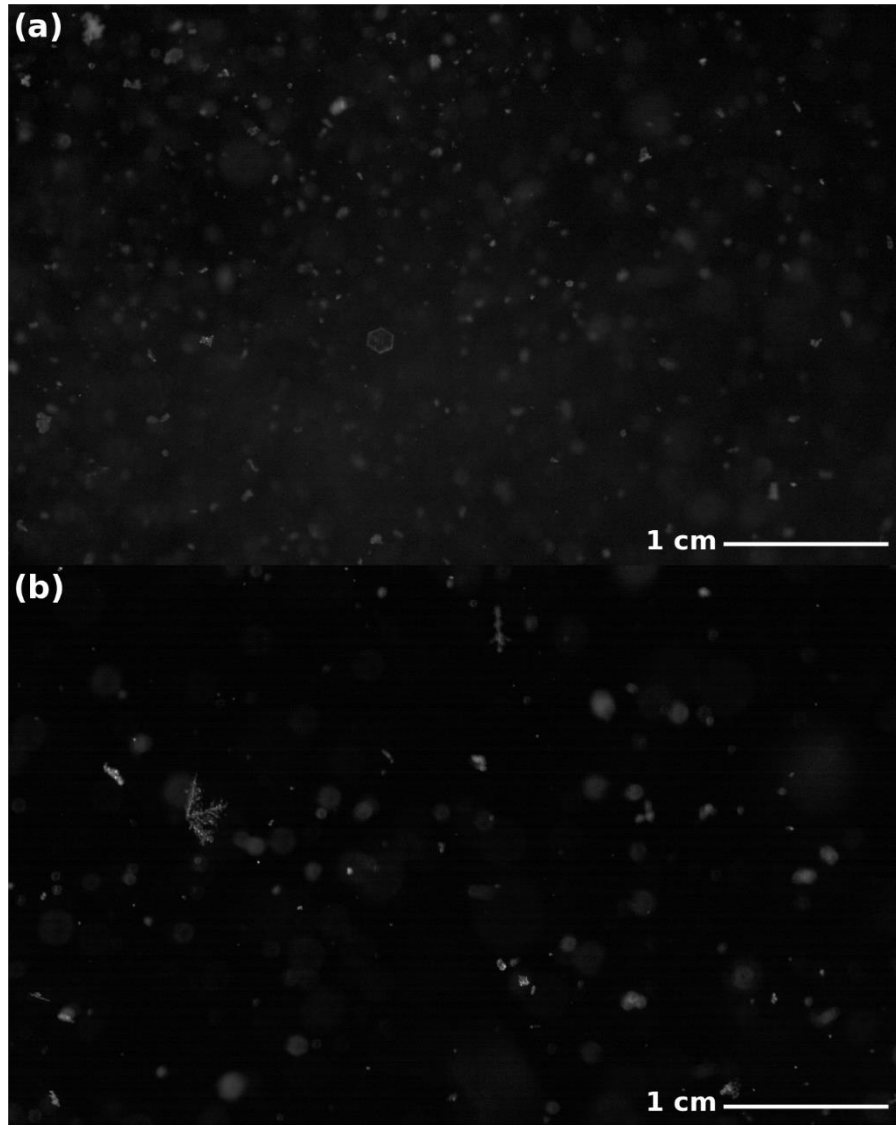


Figure 2. Singular frames from OSCRE during blizzards. Images are valid at a) 1630 UTC 29 December 2019 and b) 1010 UTC 12 February 2020.

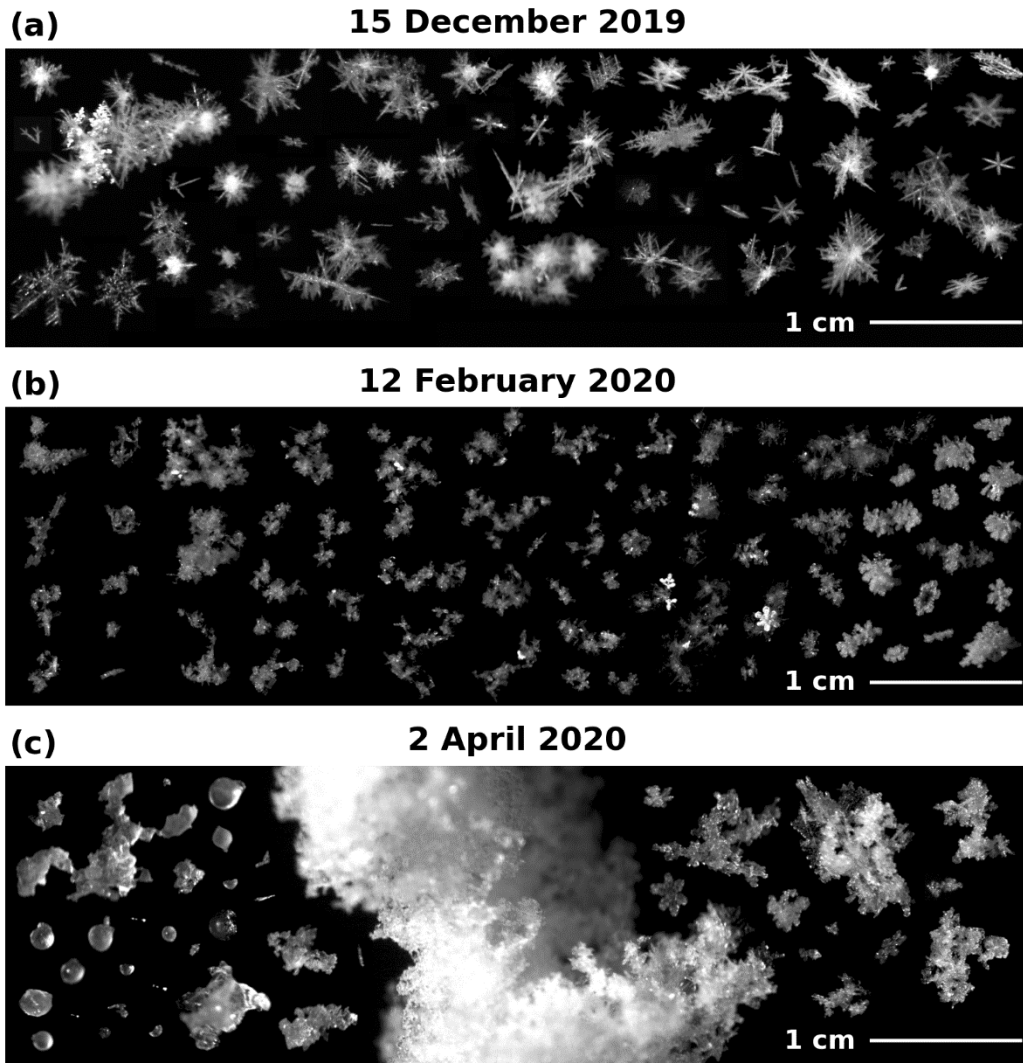


Figure 3. Composite images from OSCRE for a) 1500 – 2000 UTC 15 December 2019, b) 0500 – 0730 UTC 12 February 2020, and c) 1230 – 1330 UTC 2 April 2020. Images are arranged in approximate chronological order with earlier times on the left.

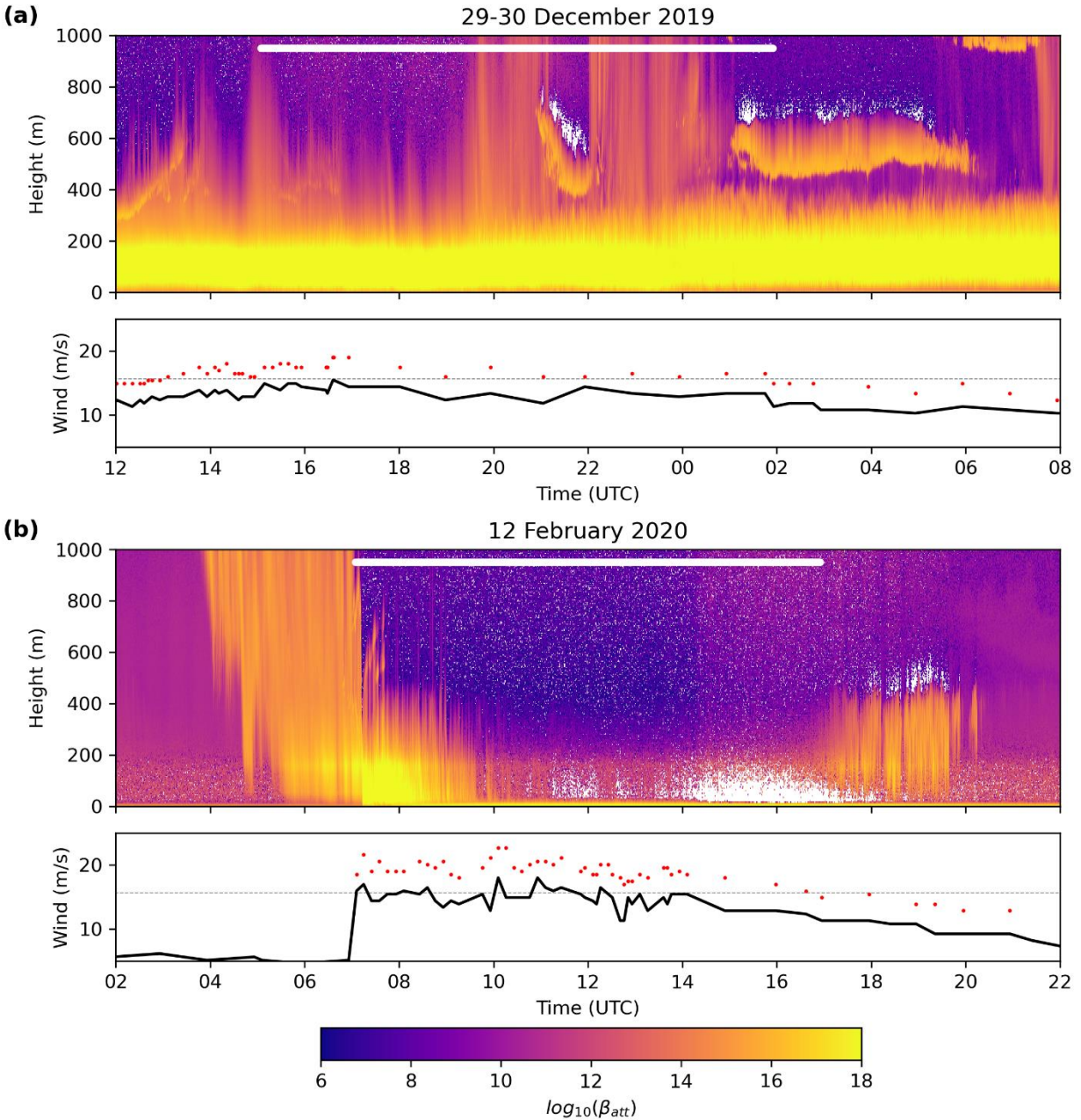


Figure 4. Time series plots of attenuated backscatter from the Lufft CHM 15K ceilometer at the Oakville Prairie Observatory and measured 10 m winds at the nearby Grand Forks, North Dakota Air Force Base (KRDR) for blizzard events on (a) 29-30 December 2019 and (b) 12 February 2020. White bars indicate time periods with visibility < 0.5 mi at KRDR. Sustained winds are plotted with black solid lines with wind gusts given by red markers. The dashed grey lines represent the threshold wind speed (15.6 m/s or 35mph) for blizzard conditions.

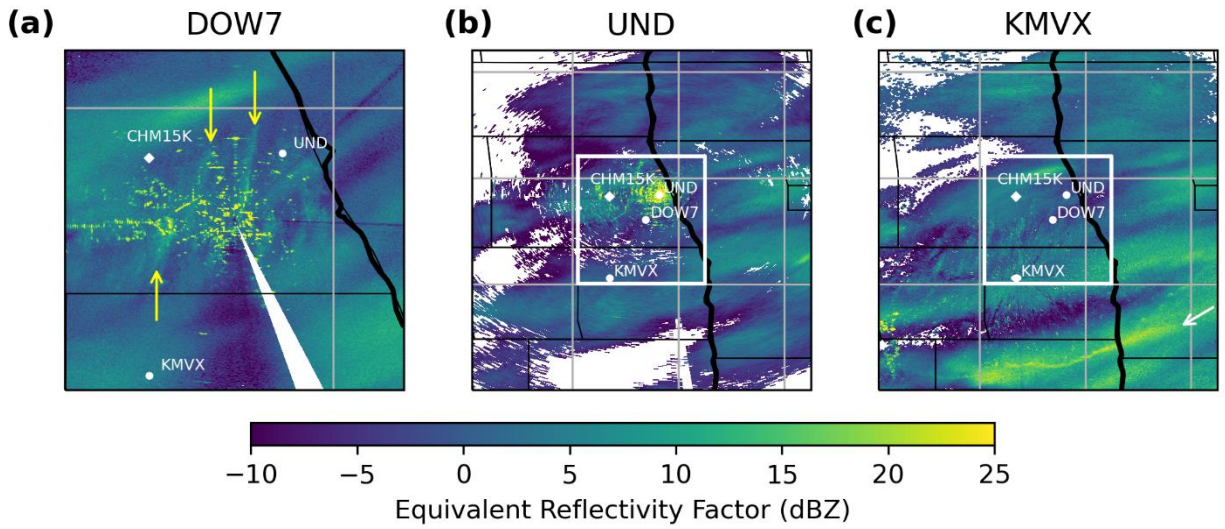


Figure 5. Reflectivity PPIs valid at 0840 UTC 12 February 2020 for a) DOW7 (1.3°), b) UND (2.0°), and c) KVMX (0.5°). DOW7 is plotted as a geographical subset as indicated by the white box. Horizontal convective rolls in the DOW7 panel are denoted by yellow arrows, while the fineline associated with the Arctic front is identified by the white arrow in the KVMX panel. CHM15K is the location of the ceilometer shown in Figure 4b.

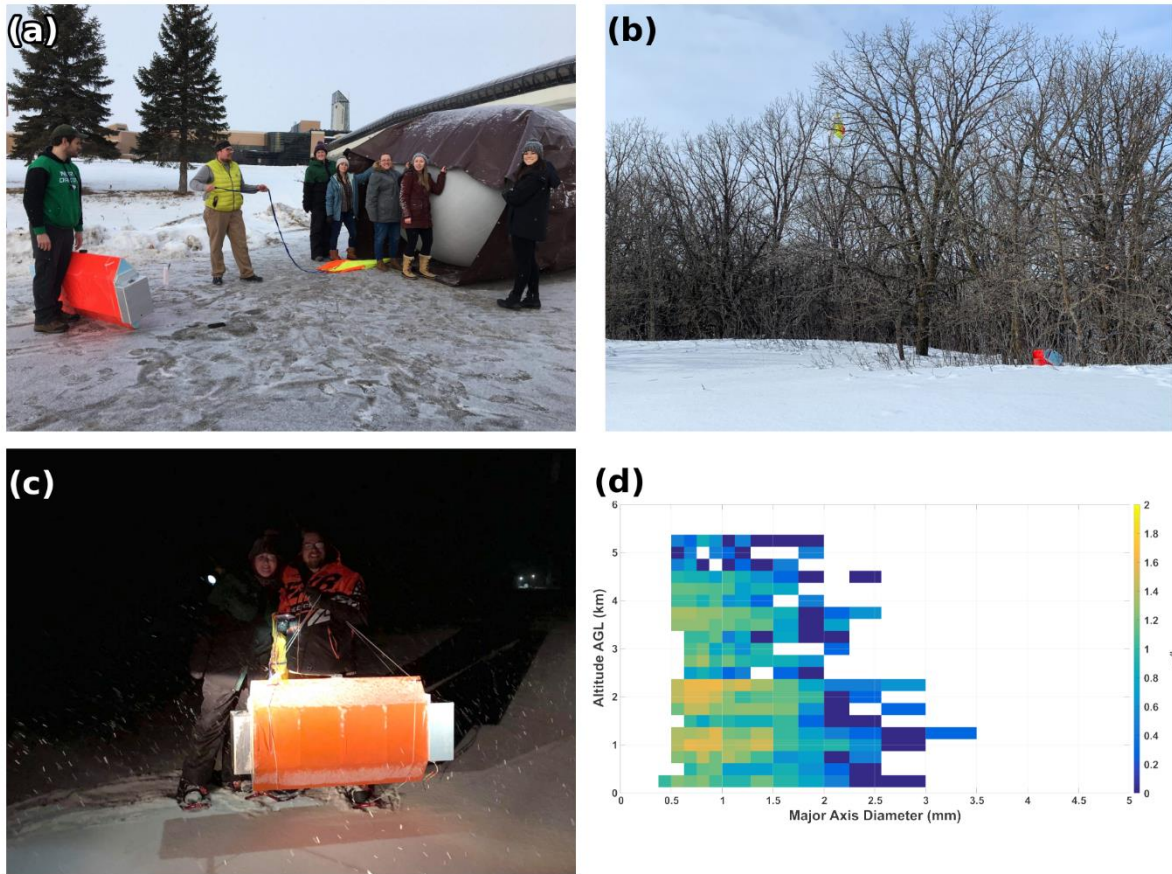


Figure 6. PASIV launches during BLOWN-UNDER: a) The initial launch is prepared during a light snow event on 6 February 2020. From left to right: Alec Szczepanski, Aaron Kennedy, Julianna Glinskas, Caitlyn Mensch, Nikki Carson-Marquis, Nicole Loeb, and Elizabeth Sims. b) The 6 February 2020 launch is recovered within the Sand Hill River Recreation Area near Fertile, Minnesota, on the same day. c) The 12 February 2020 launch is recovered by Julianna Glinskas, Aaron Kennedy, and Nicole Loeb (photographer) from a field near Key West, Minnesota, prior to the onset of blizzard conditions. d) The vertical profile of major axis diameter (mm) from the 12 February 2020 launch.

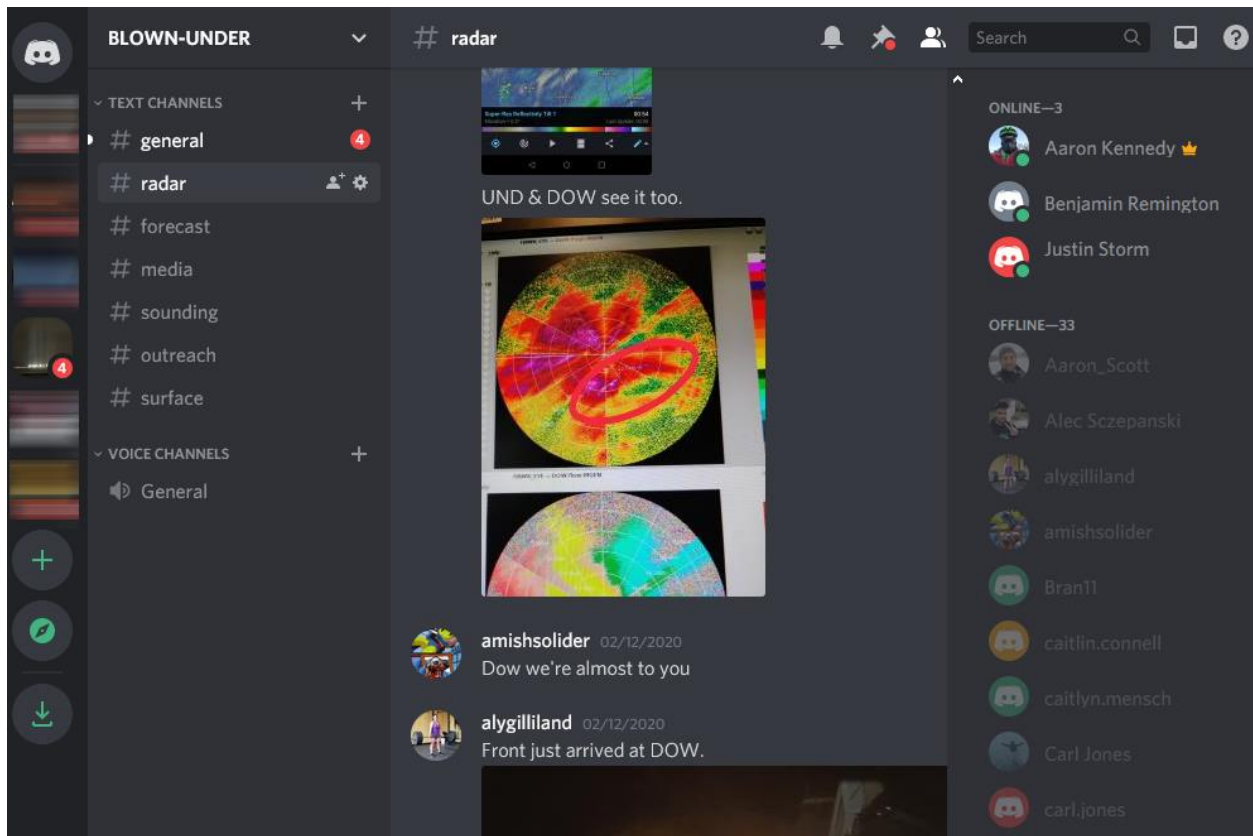


Figure 7. Example of Discord use within the #radar sub-channel during the 12 February 2020 blizzard event.

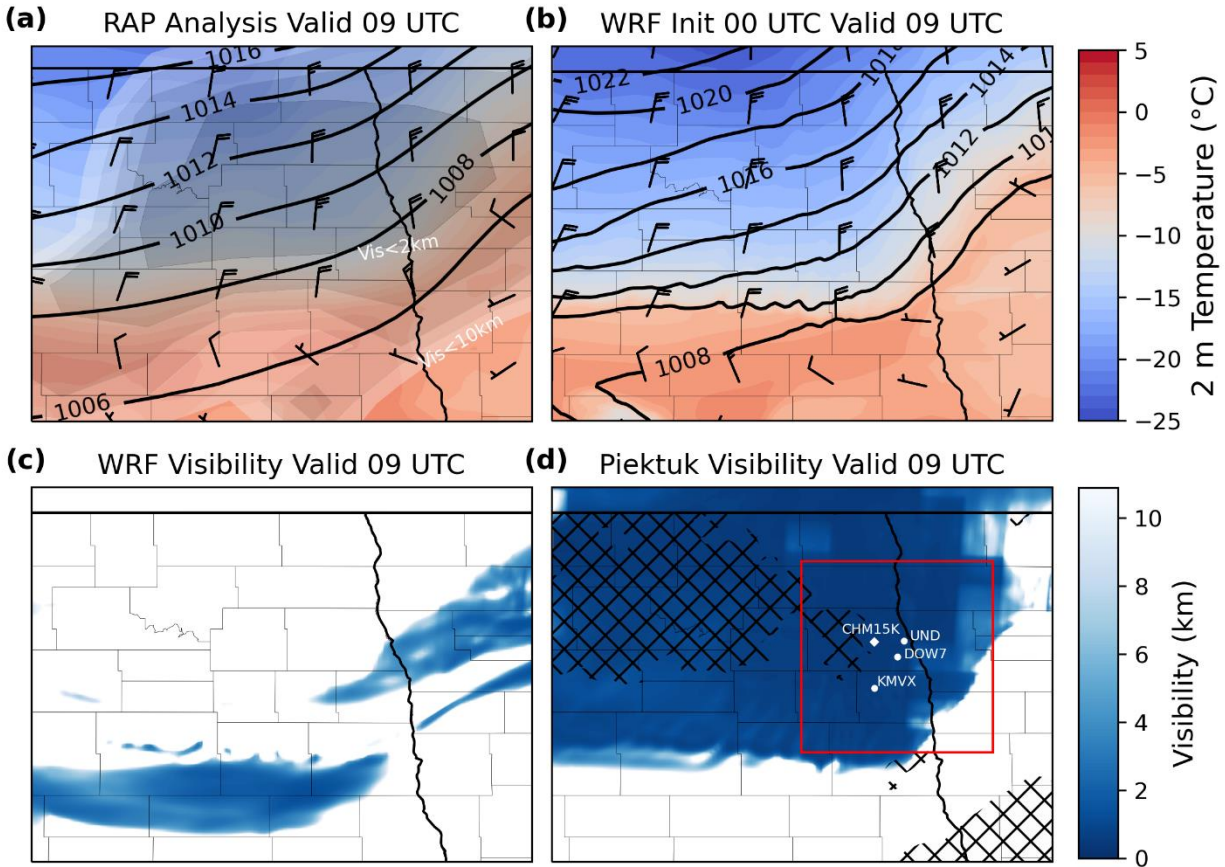


Figure 8. Analysis and forecast of 2 m temperature ($^{\circ}$ C), MSLP (mb), 10 m winds (m/s), and visibility (km) valid at 0900 UTC 12 February 2020. a) RAP analysis with observed visibilities contoured with grey shading. b) WRF 9 hr forecast initialized at 00 UTC 12 February 2020. c) WRF AFWA visibility (km). d) Piektuk blowing snow visibility (km) initialized from WRF output. The hatching in panel (d) indicates regions without recent snowfall (72 hours prior) as identified from the NOAA National Snow Analyses produced by the National Operational Hydrologic Remote Sensing Center. Red box in panel (d) indicates the area shown in Figure 5 panels (b) and (c).



Figure 9. Examples of hands-on outreach activities: a) blizzard in a box, b) atmospheric optics with a custom hexagonal ice crystal, c) snowflake habit matching, and d) snowflake art.



Figure 10. Undergraduate student Justin Storm walks away from DOW7 as the 12 February 2020 ground blizzard comes to an end. Picture taken by undergraduate student Caitlin Connell.